Journal of Physics and Chemistry of Solids 99 (2016) 105–110

Contents lists available at ScienceDirect

Journal of Physics and Chemistry of Solids

journal homepage: www.elsevier.com/locate/jpcs

High-temperature superconductivity at high pressures for $H_3Si_xP_{1-x}$, $H_3P_xS_{1-x}$, and $H_3Cl_xS_{1-x}$

F. Fan [a], D.A. Papaconstantopoulos [a], M.J. Mehl [b,*], B.M. Klein [c]

[a] Department of Computational and Data Sciences, George Mason University, Fairfax, VA 22030, USA
[b] Center for Materials Physics & Technology, U.S. Naval Research Laboratory, Washington, DC 20375, USA
[c] Department of Physics, University of California Davis, Davis, CA 95616, USA

ARTICLE INFO

Article history:
Received 22 June 2016
Received in revised form
21 July 2016
Accepted 14 August 2016
Available online 17 August 2016

Keywords:
Superconductivity
High-temperature
Hydrogen
Electronic structure

ABSTRACT

Recent experimental and computational works have established the occurrence of superconducting temperatures, T_c, near 200 K when the pressure is close to 200 GPa in hydrogen-based sulfur compounds. In this work we investigate the effects of phosphorus and chlorine substitutions of sulfur on T_c, as well as the effect of hydrogen vacancies. In addition, we explore the superconductivity-relevant parameters in the $H_3Si_xP_{1-x}$ system.

In executing this work we used the virtual crystal approximation and performed a systematic set of linearized augmented plane wave calculations (LAPW) for many different concentrations of the sulfur component. From the densities of states and the scattering phase shifts at the Fermi level, we calculated electron-ion matrix elements and estimated the electron-phonon coupling constants for different concentrations, as well as T_c. We find that the highest value of $T_c=197$ K corresponds to a phosphorus concentration of $x=0.15$, or 8.85 valence electrons in a $H_3P_{0.15}S_{0.85}$ alloy. From a detailed analysis of the results given by a Gaspari–Gyorffy (GG) determination of the Hopfield parameter, we identify the role of each term in the GG equation that produce the maximum T_c. In addition, we present a non-orthogonal tight-binding parameterization of the band structure of H_3S which fits very well with the LAPW results.

Published by Elsevier Ltd.

1. Introduction

Back in the late sixties, Ashcroft [1,2] made the bold prediction of room temperature superconductivity in metallic hydrogen under very high pressures. Later in the seventies, a quantitative evaluation of the electron-phonon (e-p) coupling [3,4] using the Gaspari–Gyorffy–McMillan (GGM) theories [5,6] supported Ashcroft's prediction. In Ref. [3] an e-p coupling $\lambda = 1.86$ gave a superconducting transition temperature $T_c=234$ K at an estimated pressure of 4.6 Mbar.

The ideas of Ashcroft have been recently confirmed by the first-principles calculations of Duan et al. [7] and the experiments of Drozdov et al. [8] that followed. A series of theoretical papers [9–15] further confirm that hydrogen-based high-temperature superconductivity is realized in the sulfur compound H_3S under 200 GPa pressure. Reference [9] presents a comprehensive set of calculations for H_3S using the GGM theory. In the present paper we pursue an extended study in this class of hydrides for compounds of the formula $H_3M_xY_{1-x}$, where M and Y represent combinations of Si, P, S, and Cl and x the concentration. We have performed band structure calculations in the virtual crystal approximation (VCA). The resulting angular-momentum components of the densities of states (DOS) at the Fermi level (E_f) and the phase shifts obtained from the computed band structure potentials are the input to the GGM theory for the evaluation of the electron-ion matrix element known as the Hopfield parameter (η).

2. Computational details

We have applied the linearized augmented plane wave (LAPW) code developed at NRL [16,17], using the Hedin–Lundqvist form of exchange and correlation, to calculate the band structure and total energy of many compositions of the $H_3M_xY_{1-x}$ system defined above. All calculations were performed in the Im $\bar{3}$m crystal structure [7] in which the occurrence of high-T_c superconductivity has been established for H_3S. We modeled the x dependence of these compounds with the VCA, i.e. we simply entered in the LAPW code an averaged atomic number Z and an averaged

* Corresponding author. Current address: Department of Physics, U.S. Naval Academy, Annapolis MD 21402, USA.
E-mail addresses: dpapacon@gmu.edu (D.A. Papaconstantopoulos), mmehl@usna.edu (M.J. Mehl).

http://dx.doi.org/10.1016/j.jpcs.2016.08.007
0022-3697/Published by Elsevier Ltd.

number of valence electrons. The total energy minimization was done using the third-order Birch equation [18]. The total and angular momentum decomposed densities of electronic states were obtained by the tetrahedron method using LAPW results on a k-point uniformly distributed grid of 1785 points in the bcc irreducible Brillouin zone to ensure very accurate convergence. Subsequently, we applied the Gaspari–Gyorffy (GG) formula to obtain the parameter η, then the Allen–Dynes modification [19] of the McMillan equation to determine T_c. The main steps here are to determine the electron–phonon coupling constant λ_j given by McMillan [6] as

$$\lambda_j = \frac{N(E_f)\langle I_j^2\rangle}{M_j\langle\omega_j^2\rangle} \equiv \frac{\eta_j}{M_j\langle w_j^2\rangle} \tag{1}$$

where $N(E_f)$ is the total DOS per spin at E_f and the index j corresponds to hydrogen and to the M-Y average phonon frequency. The Hopfield parameter η_j for the two components is computed by the GG formula shown below:

$$\eta_j = \frac{1}{N(E_f)}\sum_{l=0}^{2} 2(l+1)\sin^2\left(\delta_l^j - \delta_{(l+1)}\right)v_l^j v_{(l+1)}^j \tag{2}$$

where δ_l^j is the scattering phase shift for the j-th atom, the sum of which is related to the deformation potential, and $v_l^j = N_l^j(E_f)/N_l^{j(1)}$ is the ratio of the l-th partial DOS of the j-th atom to $N^{(1)}$, the free scatterer DOS, for the given atomic potential in a homogeneous system. The free scatterer DOS is defined as

$$N_l^{j(1)} = (2l+1)\int_0^{R_s}\left[u_l^j(r, E_f)\right]^2 r^2 dr \tag{3}$$

where u_l is the radial wave function and the upper limit of the integral is the muffin-tin radius R_s. In previous works, Eqs. (2) and (3) contain multiplying factors of E_f/π^2 and $\sqrt{E_f}/\pi$, respectively. But by examining these equations it is easy to see that these factors cancel out.

Finally, we use the Allen–Dynes equation to determine the superconducting transition temperature T_c as follows:

$$T_c = f_1 f_2 \frac{\omega_{\log}}{1.2}\exp\left[-\frac{1.04(1+\lambda)}{\lambda - \mu^*(1+0.62\lambda)}\right] \tag{4}$$

In Eq. (4) we have set the Coulomb pseudopotential $\mu^* = 0.1$ and $f_2 = 1$. f_1 is the strong coupling factor given by

$$f_1 = \left[1 + \left(\frac{\lambda}{2.46 + 9.35\mu^*}\right)^{1.5}\right]^{1/3}. \tag{5}$$

As we discuss in the next section, f_1 can provide an additional 10% enhancement to T_c. We have used the values for $\omega_{\log}$ and $\langle\omega_j^2\rangle$ found in Ref. [9] from the analysis of the results of Duan et al. (Ref. [7]). Our choice of $\mu^* = 0.1$ can be justified by the empirical formula proposed by Bennemann and Garland [20]. Indeed the low values of $N(E_f)$ shown in Table I of our Appendix are consistent with low μ^*.

3. Results

In Fig. 1 we show the Pressure vs. Volume (a) and Bulk Modulus vs. Volume (b) relationships found from the Birch fit for phosphorus concentrations $x=0.0$, 0.5, and 1.0. It is interesting that for all three concentrations, these graphs are very close to each other, with a pressure near 200 GPa at $V=87.8$ Bohr^3 (cubic lattice constant =5.6 Bohr). This is the pressure at which superconducting temperature close to 200 K has been observed, consistent with our and others' calculated values.

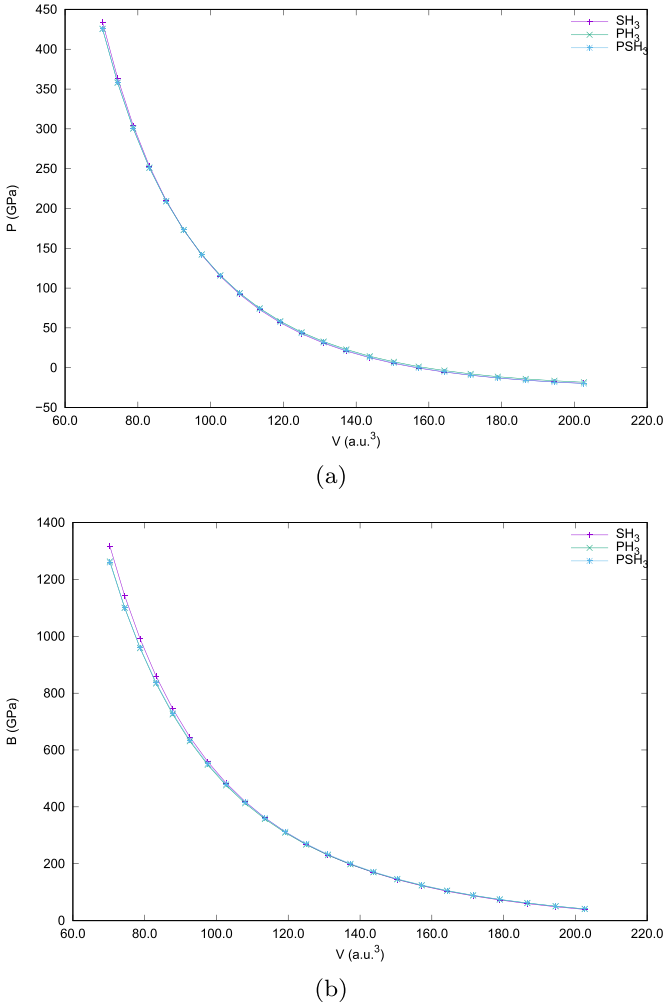

Fig. 1. (a) Pressure vs. Volume and (b) Bulk Modulus vs. Volume relationships. The red crosses (+) are for SH_3, the green X for PH_3, and the blue stars (*) are for a virtual crystal (PS)H_3 ($x=0.5$). (For interpretation of the references to color in this figure legend, the reader is referred to the web version of this article.)

Fig. 2 displays the energy bands of the 50–50 Sulfur–Phosphorus ($x=0.5$) alloy for lattice constants $a=6.8$ ($P=0$) and $a=5.6$ ($P=200$ GPa). We note that the energy bands at $P=200$ GPa have an occupied band width of 1.78 Ry, while at equilibrium the band width is 1.2 Ry. We have also found that certain bands near E_f undergo reordering of their symmetry, as is shown at the Gamma point where the state Γ_{12} under high pressure switches with the Γ_{15} (p-character). In addition, the Γ_{12} (which has d-sulfur and s-hydrogen character) has its d-character increased under pressure.

In Fig. 3 we present the total DOS for H_3S ($x=0.0$) and alloying phosphorus concentrations $x=0.5$ and $x=0.15$. We note that these DOS plots have all very similar structure, showing one peak below

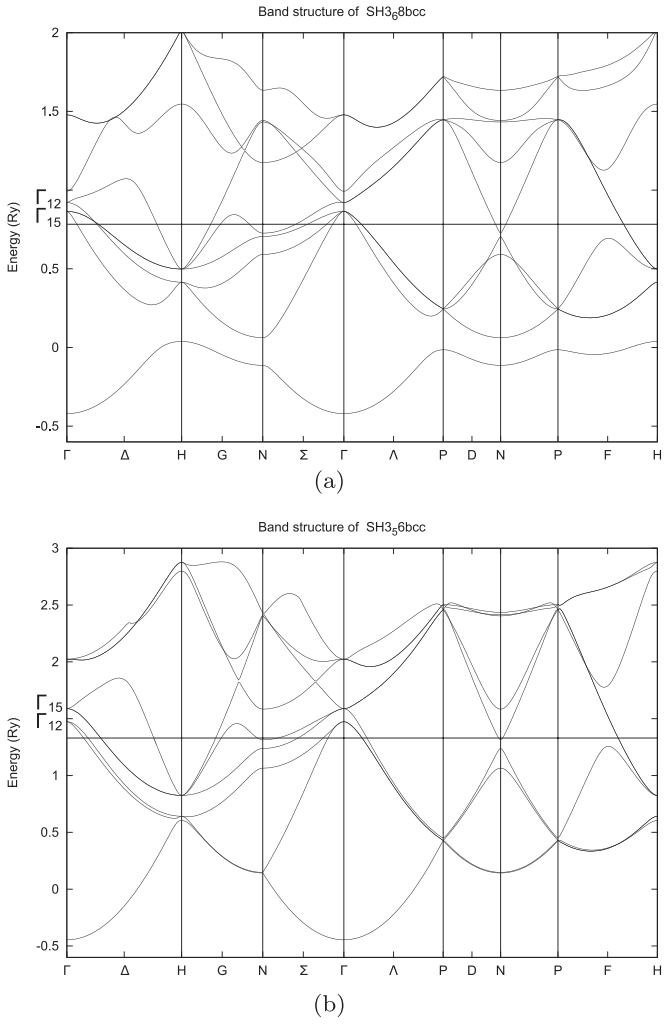

Fig. 2. Energy bands of the 50–50 Sulfur–Phosphorus ($x=0.5$) for lattice constants (a) $a=6.8$ a.u. ($P=0$) and (b) $a=5.6$ a.u. ($P=200$ GPa).

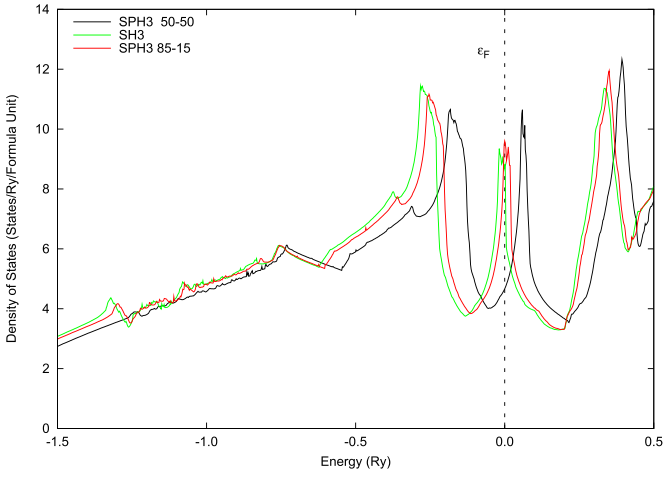

Fig. 3. Total DOS for H_3S (green line, furthest to the left) and alloying phosphorus concentrations $x=0.5$ (black line, furthest to the right) and $x=0.15$ (red line, between the other lines). (For interpretation of the references to color in this figure, the reader is referred to the web version of this article.)

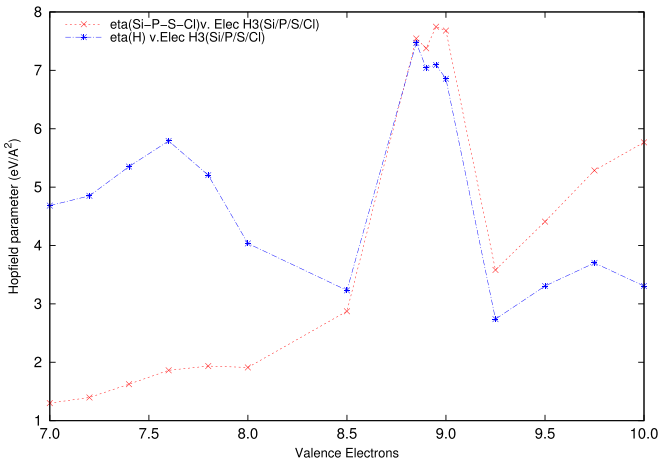

Fig. 4. Values of the Hopfield parameter η as a function of the number of valence electrons for lattice constant $a=5.6$ a.u. The red crosses (+) are for the central atom, while the green X are for hydrogen.(For interpretation of the references to color in this figure, the reader is referred to the web version of this article.)

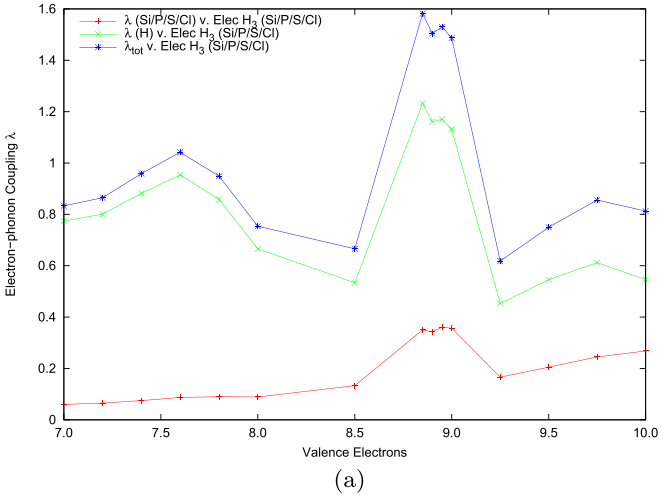

Fig. 5. Concentration (or valence electron) dependence of (a) the coupling constant λ and (b) the superconducting critical temperature T_c. In (a), the red crosses (+) are for the central atom, the green X for hydrogen, and the blue stars (*) give the total λ. (For interpretation of the references to color in this figure, the reader is referred to the web version of this article.)

E_f, one other peak very near E_f, and a third peak above E_f. We can view these peaks as Van Hove singularities. So the main difference in these DOS plots is in the position of E_f, which means that a rigid band model is applicable.

Fig. 4 plots the values of the Hopfield parameter η for the two components of the material, as a function of the number of valence electrons. It is evident that seven valence electrons correspond to H_3Si, eight electrons to H_3P, nine electrons to H_3S and ten electrons to H_3Cl. The results shown in Fig. 4 are for lattice constant $a=5.6$ Bohr and have the hydrogen component multiplied by three. We note that, approximately, these quantities reach a maximum for $x=0.1$ or 8.9 valence electrons. This suggests that we should be looking for a maximum superconducting transition temperature, T_c, near the $x=0.1$ concentration.

To quantify the above predictions we need to estimate the force constants $(M\omega^2)_j$ so that values for the electron-phonon coupling constants λ can be obtained. Using our previous analysis [9] for pure H_3S and the results of Duan et al. [7], we derive the following values of the averaged phonon frequencies in H_3S: $\langle\omega\rangle_S = 615$ K, $\langle\omega\rangle_H = 1840$ K, and $\omega_{\log} = 1560$ K. Now it is reasonable to assume that the $M\omega^2$ of H (optic mode) should be nearly constant for small variations of x near the sulfur end. The question then is how the $M\omega^2$ of the elements substituting for sulfur depends on x. This term represents the acoustic mode with a phonon frequency usually proportional to the bulk modulus B. Our calculations of B from the Birch fit at $a=5.6$ a.u. as shown in Fig. 1(b), give nearly the same value for all concentrations. Therefore, it is reasonable to conclude that both acoustic and optic phonon frequencies have weak dependence on x and hence the variation of λ with x is mainly due to the changing values of η. Fig. 5(a) and (b) show the concentration (or valence electron) dependence of the coupling constant λ and the superconducting critical temperature T_c found using Eq. (4).

A summary of our results (always for lattice constant $a=5.6$ a.u.) is given in the Appendix A Table I which also includes the effect of hydrogen vacancies, also computed in the VCA.

In the results shown in Fig. 5 we use a value of $\mu^* = 0.1$ as stated at the end of Section 2. Flores-Livas et al. [21] and Akashi et al. [22] have made estimates of μ^* which are larger than this value. Using a smaller value of μ^* would lower the value of T_c in our calculations, but the qualitative features of Fig. 5 would not be affected. The same can be said about phonon anharmonicity which, according to Errea et al. [23], lowers the calculated value of T_c.

It is interesting to note that the maximum $T_c=197$ K is found for 8.85 valence electrons which corresponds to a 15% phosphorus concentration and correlates with the Van Hove singularity in the DOS shown in Fig. 3. However the explanation of superconductivity in this material is not based on the value of $N(E_f)$, which is in fact rather low.

Our analysis is based on the assumption that the force constant $M\langle\omega^2\rangle$ in the denominator of λ remains constant partially justified in Fig. 1(b) shown the same bulk modulus dependence for different concentrations. Therefore our conclusion is that the Hopfield parameter η holds the key to understanding the high T_c found in these materials.

Now consider the variation of the Hopfield parameter in this system. Ref. [9] shows that in H_3S the dominant terms in the summation of the Gaspari–Gyorffy (GG) formula (Eq. (2)) are the *pd* channel for the sulfur component, and the *sp* channel for hydrogen. Indeed, the η_{pd} is 84% of the total sulfur contribution to η, and the η_{sp} nearly 100% of the total hydrogen shown in Table II of Appendix A. This observation holds almost exactly the same for our VCA calculations for the other concentrations. In Table II we analyze further the results obtained using the GG equation. We can see that each term of the sum is a product of three quantities as follows:

- $2(l+1)/N(E_f)$. This is a large number mainly due to the $2(l+1)$ factor and is also influenced by the denominator $N(E_f)$.
- $\sin^2\left(\delta_l^j - \delta_{(l+1)}^j\right)$. This reaches its largest values for $l=1$ in sulfur (0.58) and $l=0$ in hydrogen (0.33) for the case of $x=0.15$. In searching for even higher T_c, it would be interesting to explore ways of approaching resonance with a value close to 1.0. At this writing we do not know how to reach this limit.
- $v_l v_{(l+1)}$. This is the ratio of the l-components of the DOS at E_f over the free scatterers and reaches its largest values over one for $x=0.15$.

The last column in Table II shows the Hopfield parameter for each l confirming the strength of S-*pd* and H-*sp* channels. These should be compared with the total η given in Table I of Appendix A.

We have also ruled out the possibility of magnetism in these materials by calculating the Stoner criterion using the approach of Vosko and Perdew [24]. We found a very low value, 0.045, for H_3S.

4. Tight-binding fit

Lastly, we present a non-orthogonal tight-binding (TB) fit for the prototype compound H_3S at lattice constant $a=5.6$ a.u. This TB fit follows the Naval Research Laboratory tight-binding (NRL-TB) method, where the on-site terms of the Hamiltonian are written as a polynomial, which is a function of atom density, and the hopping and overlap non-diagonal terms are polynomial functions of the interatomic distance R. The size of the Hamiltonian is a 12×12 matrix including the *s*, *p*, and *d* orbitals of sulfur and three *s* hydrogen orbitals. We have fitted 6 LAPW bands for 55 k-points in the irreducible bcc Brillouin zone with an RMS fitting error of 10 mRy. The comparison of LAPW and TB energy bands is given in Fig. 6 which shows excellent agreement. Note that the fit was performed on the uniformly distributed 55 k-point grid and not

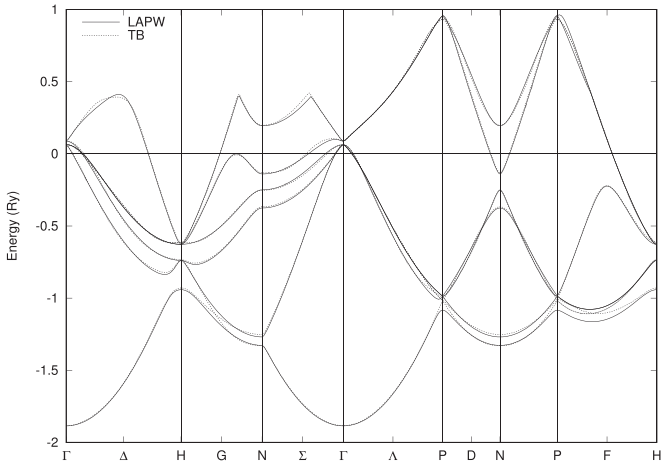

Fig. 6. Graphical comparison of LAPW (solid line) results with the tight-binding fit (dashed line) for H_3S at $a=5.6$ a.u.

along the symmetry lines of Fig. 6. In Appendix B we list the relevant equations of the NRL-TB method and the coefficients of the expansion polynomials used. A Slater–Koster fit was recently presented by Quan and Pickett [13] and by Ortenzi et al [25]. The details are different than in our approach and direct comparison can not be made. However, we note that in our TB fit we have included the sulfur *d*-orbitals; we believe they are important for the compressed lattice. We note that although in Fig. 6 we have placed the Fermi level at zero, in Table III our on-site parameters h_l refer to E_f=1.326 Ry.

5. Summary and conclusions

It is well known that the most important parameter entering the Allen-Dynes, or any other McMillan-like equation, for determining the superconducting transition temperature is the electron-phonon coupling constant λ. The value of λ as given in Eq. (1) is a result of a delicate balance between the Hopfield parameter η and the force constant $M\langle\omega^2\rangle$. In the case of the H_3SP alloys we have studied here the relative small $M\langle\omega^2\rangle$, especially for the hydrogen sites, is an important ingredient in obtaining large values of λ. However, a value of η exceeding 7 eV/Å^2 is essential to give values of λ above 1.5. In this work we have concluded that for phosphorus compositions between 0 and 0.2 both the S-P and H sites (optic modes) must have nearly constant force constants because the hydrogen composition remains the same, and for the S-P sites (acoustic modes) we found the bulk modulus essentially unchanged as a function of composition. Therefore, the high values and variation of λ and hence T_c at the high S content are mainly due to the corresponding large values of η on both sites. Studying the Gaspari–Gyorffy formula we found that these high values of η come from the *pd* channel of S-P and from the *sp* channel of H. We also emphasize that the η are large because of large electron-matrix elements $\langle I^2\rangle$ and not because of $N(E_f)$ which has quite modest values around E_f (~4.5 states/Ry/spin). Finally, we point out that the position of E_f with respect to the Van Hove singularity is not crucial for the occurrence of superconductivity in these materials. In other words, T_c over 180 K can be obtained without E_f falling exactly on the singularity peak.

We also present a non-orthogonal tight-binding fit which is in nearly perfect agreement with the LAPW band structure for the highest pressure lattice constant, a=5.6 a.u.

Acknowledgments

We acknowledge useful discussions with W.E. Pickett. This work was partially supported by U. S. Naval Research Laboratory grant N00173-11-1-G002 and U.S. Department of Energy grant DE-SC0014337. MJM is supported by the U.S. Office of Naval Research.

Appendix A

See Tables A.1 and A.2 .

Table A.1
Summary of the key parameters leading to high temperature superconductivity at the lattice parameter a=5.6 a.u. The units of $N(E_f)$ are States/Ry/Spin.

Val. elec.	$N(E_f)$	η (S)	η (H) (eV/Å^2)	λ (S)	λ (H)	λ (tot)	T_c (K)
7.00 (Si)	3.229	1.301	1.561	0.060	0.258	0.833	79
7.20	3.522	1.397	1.617	0.065	0.267	0.865	85
7.40	4.144	1.625	1.784	0.075	0.294	0.959	102
7.60	4.747	1.863	1.930	0.087	0.318	1.042	117
7.80	4.429	1.935	1.735	0.090	0.286	0.949	101
8.00 (P)	3.548	1.912	1.345	0.089	0.222	0.754	64
8.50	2.333	2.874	1.077	0.133	0.178	0.666	47
8.85	4.798	7.545	2.490	0.350	0.411	1.582	197
8.90	4.518	7.378	2.347	0.343	0.387	1.504	187
8.95	4.568	7.746	2.364	0.360	0.390	1.530	190
9.00 (S)	4.389	7.680	2.285	0.357	0.377	1.487	185
9.25	1.651	3.581	0.913	0.166	0.151	0.618	38
9.50	1.942	4.409	1.102	0.205	0.182	0.750	63
9.75	2.218	5.285	1.234	0.245	0.204	0.856	84
10.00 (Cl)	1.971	5.767	1.102	0.268	0.182	0.813	75
H vacancy							
8.91	4.494	7.858	2.167	0.365	0.358	1.437	178
8.94	4.571	8.021	2.249	0.372	0.371	1.485	184
8.97	4.432	7.764	2.245	0.360	0.370	1.472	183

Table A.2
Analysis of the results obtained from the GG equation.

l	$2(l+1)/N(E_f)$	$\sin^2(\delta_l^j - \delta_{(l+1)}^j)$	$v_l v_{(l+1)}$	η (eV/Å^2)
H_3PS (8.5 valence electrons x=0.5)				
Sulfur site				
0	11.659	0.138	0.207	0.333
1	23.318	0.390	0.262	2.380
2	34.977	0.021	0.218	0.161
Hydrogen site				
0	11.659	0.329	0.279	1.073
H_3PS (8.85 valence electrons x=0.15)				
Sulfur site				
0	5.663	0.157	1.049	0.934
1	11.326	0.520	1.060	6.243
2	17.007	0.024	0.905	0.367
Hydrogen site				
0	5.663	0.332	1.319	2.483
H_3S (9.0 valence electrons x=0.0)				
Sulfur site				
0	6.197	0.164	0.834	0.850
1	12.395	0.577	0.907	6.481
2	18.592	0.024	0.767	0.348
Hydrogen site				
0	6.197	0.333	1.104	2.279

Appendix B. Non-orthogonal tight-binding fit for H_3S at a=5.6 a.u

See Table B.3 .

Table B.3
Tight-binding parameters for H_3S. On-site energies are generated from the densities of S and H atoms: $\rho_S = \Sigma_S \exp\left(-\lambda_S^2 R\right) F(R)$ where $\lambda_S = 0.98485$ a. u.$^{-1/2}$ and $\rho_H = \Sigma_H \exp\left(-\lambda_H^2 R\right) F(R)$ where $\lambda_H = 1.00054$ a. u.$^{-1/2}$. $F(R)$ is the cutoff function with $R_c = 8.5$ a.u. and $L_c = 0.5$ a.u. All energies are in Rydberg, all distances in a.u.

On-site parameters

S–S interactions

$h_l = a_l + b_l \rho_S^{2/3} + c_l \rho_S^{4/3} + d_l \rho_S^2$

l	a_l	b_l	c_l	d_l	h_l
s	−0.34850	0.94205	5.08243	26.8771	0.20980
p	1.49723	−0.59703	−2.97881	−15.0358	1.16646
t_{2g}	1.45907	1.26778	6.58257	34.1830	2.18688
e_g	1.47566	1.35280	7.01792	36.4118	2.25160

H–H interactions

$h_l = a_l + b_l \rho_H^{2/3} + c_l \rho_H^{4/3} + d_l \rho_H^2$

l	a_l	b_l	c_l	d_l	h_l
s	3.09151	−1.13181	−1.69161	−2.53673	1.19139

Hopping terms

$H_{ll'u}(R) = \left(e_{ll'u} + f_{ll'u} R + g_{ll'u} R^2\right) \exp\left(-q_{ll'u}^2 R\right) F(R)$

S–S interactions

$H_{ll'u}$	$e_{ll'u}$	$f_{ll'u}$	$g_{ll'u}$	$q_{ll'u}$
$H_{ss\sigma}$	−37.2642	−1.97590	0.89465	1.08771
$H_{sp\sigma}$	−414.191	247.473	−119.405	1.42523
$H_{pp\sigma}$	19.0311	0.35955	−0.62591	0.78886
$H_{pp\pi}$	−884.237	−6.52298	43.2797	1.26562
$H_{sd\sigma}$	−13,603.8	6224.48	−704.485	1.25091
$H_{pd\sigma}$	−22.9207	−0.06584	1.05093	0.80785
$H_{pd\pi}$	−83.5738	−2.85547	3.33988	1.07239
$H_{dd\sigma}$	−144.566	0.92839	7.62901	1.00021
$H_{dd\pi}$	7.48462	−0.40269	−0.36198	0.80406
$H_{dd\delta}$	23.4424	0.08891	−0.88232	0.88811

H–H interactions

$H_{ll'u}$	$e_{ll'u}$	$f_{ll'u}$	$g_{ll'u}$	$q_{ll'u}$
$H_{ss\sigma}$	−2.98435	2.06735	−0.28382	1.14491

S–H interactions

$H_{ll'u}$	$e_{ll'u}$	$f_{ll'u}$	$g_{ll'u}$	$q_{ll'u}$
$H_{ss\sigma}$	–26.8093	−2.02657	0.87008	1.31034
$H_{ps\sigma}$	9.45253	1.29018	−0.43811	1.10763
$H_{ds\sigma}$	103.406	29.8493	4.29253	1.46836

Overlap terms

$O_{ll'u}(R) = \left(\bar{e}_{ll'u} + \bar{f}_{ll'u} R + \bar{g}_{ll'u} R^2\right) \exp\left(-\bar{q}_{ll'u}^2 R\right) F(R)$

S–S interactions

$O_{ll'u}$	$\bar{e}_{ll'u}$	$\bar{f}_{ll'u}$	$\bar{g}_{ll'u}$	$\bar{q}_{ll'u}$
$O_{ss\sigma}$	1590.52	95.0387	−31.6272	1.45318
$O_{sp\sigma}$	5.77673	−0.10276	−0.25169	0.85220
$O_{pp\sigma}$	2.30265	0.27908	0.03186	0.89528
$O_{pp\pi}$	32.7932	3.79298	0.07538	1.18144
$O_{sd\sigma}$	4.73694	−0.00629	−0.17353	0.65696
$O_{pd\sigma}$	−2.57262	−0.00631	0.08985	0.49286
$O_{pd\pi}$	−19.4197	−0.32040	0.68785	0.97495
$O_{dd\sigma}$	25.9945	2.80163	0.02450	0.99923
$O_{dd\pi}$	7.50459	−0.52028	−0.69325	1.01232
$O_{dd\delta}$	−1.85436	0.04290	0.04944	0.61948

H–H interactions

$O_{ll'u}$	$\bar{e}_{ll'u}$	$\bar{f}_{ll'u}$	$\bar{g}_{ll'u}$	$\bar{q}_{ll'u}$
$O_{ss\sigma}$	1.73987	0.02241	−0.10378	0.78497

S–H interactions

$O_{ll'u}$	$\bar{e}_{ll'u}$	$\bar{f}_{ll'u}$	$\bar{g}_{ll'u}$	$\bar{q}_{ll'u}$
$O_{ss\sigma}$	0.87017	−0.05408	−0.03101	0.72466
$O_{ps\sigma}$	–1.61914	−0.16074	0.12725	0.84020
$O_{ds\sigma}$	−30.8166	4.81441	3.85248	1.24436

References

[1] N.W. Ashcroft, Metallic hydrogen a high-temperature superconductor? Phys. Rev. Lett. 21 (1968) 1748–1749, http://dx.doi.org/10.1103/PhysRevLett.21.1748.

[2] N.W. Ashcroft, Hydrogen dominant metallic alloys high temperature superconductors? Phys. Rev. Lett. 92 (2004) 187002, http://dx.doi.org/10.1103/PhysRevLett.92.187002.

[3] D.A. Papaconstantopoulos, B.M. Klein, Electron-phonon interaction and superconductivity in metallic hydrogen, Ferroelectrics 16 (1) (1977) 307–310, http://dx.doi.org/10.1080/00150197708237185.

[4] D.A. Papaconstantopoulos, L.L. Boyer, B.M. Klein, A.R. Williams, V.L. Morruzzi, J. F. Janak, Calculations of the superconducting properties of 32 metals with $z \leq 49$, Phys. Rev. B 15 (1977) 4221–4226, http://dx.doi.org/10.1103/PhysRevB.15.4221.

[5] G.D. Gaspari, B.L. Gyorffy, Electron-phonon interactions, *d* resonances, and superconductivity in transition metals, Phys. Rev. Lett. 28 (1972) 801–805, http://dx.doi.org/10.1103/PhysRevLett.28.801.

[6] W.L. McMillan, Transition temperature of strong-coupled superconductors, Phys. Rev. 167 (1968) 331–344, http://dx.doi.org/10.1103/PhysRev.167.331.

[7] D. Duan, Y. Liu, F. Tian, D. Li, X. Huang, Z. Zhao, H. Yu, B. Liu, W. Tian, T. Cui, Pressure-induced metallization of dense $(H_2S)_2H_2$ with high-tc superconductivity, Sci. Rep. 4 (2014) 6968.

[8] A.P. Drozdov, M.I. Eremets, I.A. Troyan, V. Ksenofontov, S.I. Shylin, Conventional superconductivity at 203 K at high pressures in the sulfur hydride system, Nature 525 (7567) (2015) 73–76 (letter).

[9] D. Papaconstantopoulos, B.M. Klein, M.J. Mehl, W.E. Pickett, Cubic H_3S around 200 gpa an atomic hydrogen superconductor stabilized by sulfur, Phys. Rev. B 91 (2015) 184511.

[10] N. Bernstein, C.S. Hellberg, M.D. Johannes, I.I. Mazin, M.J. Mehl, What superconducts in sulfur hydrides under pressure and why, Phys. Rev. B 91 (2015) 060511, http://dx.doi.org/10.1103/PhysRevB.91.060511.

[11] I. Errea, M. Calandra, C.J. Pickard, J. Nelson, R.J. Needs, Y. Li, H. Liu, Y. Zhang, Y. Ma, F. Mauri, High-pressure hydrogen sulfide from first principles a strongly anharmonic phonon-mediated superconductor, Phys. Rev. Lett. 114 (2015) 157004, http://dx.doi.org/10.1103/PhysRevLett.114.157004.

[12] José A. Flores-Livas, Antonio Sanna, and E. K. U. Gross, High temperature superconductivity in sulfur and selenium hydrides at high pressure, European Physical Journal B 89:63, (2016), http://dx.doi.org/10.1140/epjb/e2016-70020-0.

[13] Y. Quan, W.E. Pickett, Van Hove singularities and spectral smearing in high-temperature superconducting H_3S, Phys. Rev. B 93 (2016) 104526, http://dx.doi.org/10.1103/PhysRevB.93.104526.

[14] Y. Li, J. Hao, H. Liu, Y. Li, Y. Ma, The metallization and superconductivity of dense hydrogen sulfide, J. Chem. Phys. 140, 174712 (2014), http://dx.doi.org/10.1063/1.4874158.

[15] A. Bianconi, T. Jarlborg, Lifshitz transitions and zero point lattice fluctuations in sulfur hydride showing near room temperature superconductivity, Novel Superconducting Materials 1, 37-49 (2015), http://dx.doi.org/10.1515/nsm-2015-0006.

[16] D.J. Singh, Plane Waves, Pseudopotentials, and The LAPW Method, Kluwer Academic Publishers, Boston, 1994.

[17] The NRL LAPW code, [S.-H. Wei, H. Krakauer, Local-Density-Functional Calculation of the Pressure-Induced Metallization of BaSe and BaTe, Phys. Rev. Lett. 55, 1200-1203 (1985), http://dx.doi.org/10.1103/PhysRevLett.55.1200; D. Singh, Ground-state properties of lanthanum: Treatment of extended-core states, Phys. Rev. B 43, 6388-6392 (1991), http://dx.doi.org/10.1103/PhysRevB.43.6388.] was used with Hedin-Lundqvist exchange-correlation. DOS results were generated from 1785 K points in the irreducible Brillouin zone with the tetrahedron method. Total energies were fit to the Birch equation to obtain the P(V) equation of state.

[18] F. Birch, Finite strain isotherm and velocities for single-crystal and polycrystalline NaCl at high pressures and 300 K, J. Geophys. Res.: Solid Earth 83 (B3) (1978) 1257–1268, http://dx.doi.org/10.1029/JB083iB03p01257.

[19] P.B. Allen, R.C. Dynes, Transition temperature of strong-coupled superconductors reanalyzed, Phys. Rev. B 12 (1975) 905–922, http://dx.doi.org/10.1103/PhysRevB.12.905.

[20] K.H. Bennemann, J.W. Garland, Theory for superconductivity in d-band metals, in: Proceedings of AIP Conference, 4 (1972) 103–137. http://dx.doi.org/10.1063/1.2946179.

[21] J.A. Flores-Livas, M. Amsler, C. Heil, A. Sanna, L. Boeri, G. Profeta, C. Wolverton, S. Goedecker, E.K.U. Gross, Superconductivity in metastable phases of phosphorus-hydride compounds under high pressure, Phys. Rev. B 93 (2016) 020508, http://dx.doi.org/10.1103/PhysRevB.93.020508.

[22] R. Akashi, M. Kawamura, S. Tsuneyuki, Y. Nomura, R. Arita, First-principles study of the pressure and crystal-structure dependences of the superconducting transition temperature in compressed sulfur hydrides, Phys. Rev. B 91 (2015) 224513, http://dx.doi.org/10.1103/PhysRevB.91.224513.

[23] I. Errea, M. Calandra, C.J. Pickard, J.R. Nelson, R.J. Needs, Y. Li, H. Liu, Y. Zhang, Y. Ma, F. Mauri, Quantum hydrogen-bond symmetrization in the superconducting hydrogen sulfide system, Nature 532 (2016) 81–84, http://dx.doi.org/10.1038/nature17175.

[24] S.H. Vosko, J.P. Perdew, Theory of the spin susceptibility of an inhomogeneous electron gas via the density functional formalism, Can. J. Phys. 53 (14) (1975) 1385–1397, http://dx.doi.org/10.1139/p75-176.

[25] L. Ortenzi, E. Cappelluti, L. Pietronero, Band structure and electron-phonon coupling in H$_3$S: A tight-binding model, Phys. Rev. B 94, 064507 (2015), http://dx.doi.org/10.1103/PhysRevB.94.064507.